Nano Research
https://doi.org/10.1007/s12274-017-1807-9
Research Article
ISSN 1998-0124
CN 11-5974/O4

Copper nanowire-TiO_2-polyacrylate composite electrodes with high conductivity and smoothness for flexible polymer solar cells

Haitao Zhai[1,2], Yang Li[3], Liwei Chen[3], Xiao Wang[1,2], Liangjing Shi[1], Ranran Wang[1] (✉), and Jing Sun[1] (✉)

[1] *The State Key Lab of High Performance Ceramics and Superfine Microstructure, Shanghai Institute of Ceramics, Chinese Academy of Sciences, 1295 Dingxi Road, Shanghai 200050, China*
[2] *University of Chinese Academy of Sciences, 19 Yuquan Road, Beijing 100049, China*
[3] *Suzhou Institute of Nano-tech and Nano-bionics, Chinese Academy of Sciences, 398 Ruoshui Road, Suzhou 215123, China*

Received: 8 May 2017
Revised: 15 August 2017
Accepted: 18 August 2017

KEYWORDS
copper nanowires, transparent electrode, flexible polymer solar cells

ABSTRACT

Copper nanowire (Cu NW) transparent electrodes have attracted considerable attention due to their outstanding electrical properties, flexibility and low cost. However, complicated post-treatment techniques are needed to obtain good electrical conductivity, because of the organic residues and oxide layers on the surface of the Cu NWs. In addition, commonly used methods such as thermal annealing and acid treatment often lead to nanowire damage. Herein, a TiO_2 sol treatment was introduced to obtain Cu NW transparent electrodes with superb performance (13 Ω/sq @ 82% T) at room temperature within one minute. Polymer solar cells with excellent flexibility were then fabricated on the copper nanowire-TiO_2-polyacrylate composite electrode. The power conversion efficiency (PCE) of the cells based on a blend of poly(3-hexylthiophene) (P3HT) and phenyl-C_{61}-butyric acid methyl ester ($PC_{61}BM$) reached 3.11%, which was better than the control devices that used indium tin oxide (ITO)-PET electrodes, and outperforms other Cu NW based organic solar cells previously reported. The PCE of the solar cells based on Cu NW electrodes remained at 90% after 500 cycles of bending, while the PET/ITO solar cells failed after 20 and 200 cycles, with sheet resistance of 35 and 15 Ω/sq, respectively.

1 Introduction

Polymer solar cells (PSCs) are under intensive investigation for applications in renewable energy due to their advantageous properties of convenient fabrication, mechanical flexibility, and low cost [1–4]. Further progress in power conversion efficiency (PCE) is expected with the innovative new materials continuously being developed, along with improved manufacturing processes and device architectures [5–12]. Specifically, great effort has been made to realize lower fabrication costs [13–15]. For example, fabricating the devices on

Address correspondence to Ranran Wang, wangranran@mail.sic.ac.cn; Jing Sun, jingsun@mail.sic.ac.cn

plastic or metal foil substrates would allow roll-to-roll processing, which would significantly lower the production cost. In addition, the mechanic flexibility of the resulting devices can also potentially reduce the installation cost. Indium tin oxide (ITO) is a widely used transparent electrode in polymer solar cells. However, because of the unreliable supply of indium, the price of ITO has increased in recent years. In addition, ITO is typically coated on glass substrates, limiting its flexibility, increasing its weight, and raising the cost of the PSCs. Unfortunately, ITO coated on polymer substrates is not sufficiently conductive for solar cell applications. Due to the intrinsic brittleness of ITO, PSCs fabricated on ITO/polymer have very limited flexibility. Also, roll-to-roll fabrication techniques are not suitable for processing ITO/glass or ITO/polymer substrates.

Several candidate materials have been examined to replace ITO as flexible transparent electrodes including conducting polymers, carbon nanotubes, graphene, and metallic nanowires [16–21]. Metal nanowires, such as silver nanowires (Ag NWs) and copper nanowires (Cu NWs), have been used to form high quality electrodes. PSCs, small molecule solar cells and OLEDs have been successfully fabricated based on these metal nanowire electrodes. Song et al. [22] prepared PSCs using solution-processed Ag NW electrodes and obtained power conversion efficiencies comparable to ITO based devices. Sachse et al. [23] reported a modified lamination of an Ag NW top electrode, which resulted in a PCE of 2.1%. Li et al. [24] fabricated high-performance blue, green and red OLEDs based on Ag NW-polymer composite electrodes, which had higher electroluminescent performance than the control ITO/glass device. Although much progress has been made, silver is a noble metal and is relatively expensive. Compared with silver, copper has comparable conductivity but a much lower cost and is more readily available. Thus, replacing Ag NWs with Cu NWs should offer comparable levels of performance at a lower cost. However, the power conversion efficiencies of solar cells using Cu NW electrodes have been inferior to cells using Ag NWs in the devices produced to date. Chen et al. [25] prepared PSCs using solution-processed Cu NW electrodes and obtained a PCE of 1.4%. Despite outstanding optical and electrical properties, Cu NW electrodes have some inherent shortcomings compared with Ag NWs, such as complicated post-treatment techniques necessary to obtain good electrical conductivity and significant surface roughness. Annealing is the most commonly used technique for removing residual organic molecules and oxide layers. However, the annealing process usually involves high temperatures and H_2, which are not suitable for large-scale fabrication of flexible electrodes.

Herein, we developed a solution process to produce Cu NW transparent electrode with high conductivity at room temperature within one minute. Compared with traditional thermal annealing process, the TiO_2 sol treatment saves time and energy and is more suitable for the fabrication of flexible devices. A self-prepared TiO_2 nanoparticle sol was spin coated onto Cu NW thin films, which removes residual organic molecules and oxide layers effectively, leading to a significant decrease in the contact resistance between neighboring nanowires. Compared with the traditional thermal annealing process, the TiO_2 sol treating process is more time and energy saving. An *in situ* polymerization method was used to decrease the surface roughness of the Cu NW based electrodes. After that, the Cu NW transparent electrodes were modified with a poly(3,4-ethylene dioxythiophene):poly(styrenesulfonate) (PEDOT:PSS, PH1000) layer to further improve their surface roughness. Inverted PSCs with Cu NW based electrodes were fabricated and exhibited a PCE of 3.11% with the poly(3-hexylthiophene):[6,6]-phenyl-C_{61} butyric acid methyl ester (P3HT:PCBM) blend film as the active layer, which is better than commercial PET/ITO. In addition, the PCE of the solar cells based on Cu NW electrodes was maintained at 90% of the original value after 500 bending tests, while PET/ITO solar cells failed after 20 and 200 cycles with sheet resistances of 35 and 15 Ω/sq, respectively.

2 Experimental

2.1 Preparation of Cu NWs

For Cu NW synthesis, we used a modified self-catalytic method which has been described in detail elsewhere [26–29]. Briefly, 10 mL of oleylamine (OA) and 0.5 g of cetrimonium bromide (CTAB) were dissolved in a

glass vial at 180 ˚C. Then, 200 mg copper acetylacetonate ($Cu(acac)_2$) was added and mixed until evenly distributed. After that, 5–7 μL of a Pt nanoparticle suspension was added as catalyst. The Pt nanoparticles were synthesized as follows: 2 mg of platinous chloride was dispersed into 1.2 mL of ethylene glycol, then added to 2.3 mL of ethylene glycol and kept at 160 ˚C for 90 s. The mixture was then maintained at 180 ˚C for 12 h, resulting in the formation of red cotton-like sheets settled at the bottom of the vial. After rinsing with toluene several times, the nanowires were stored in toluene.

2.2 Preparation of the Cu NW transparent electrodes

Cu NWs were dispersed in toluene by bath sonication for 1–2 min, and then filtered with a nitrocellulose filter membrane. After filtration, the filter membranes were transferred onto a glass slide film, dried under vacuum at 80 ˚C for 2 h, and then dipped in acetone for 30 min to dissolve the filter membrane, leaving Cu NW based thin films on the glass slide. The self-prepared TiO_2 nanoparticle sol was then spin-coated onto the thin films. Then the Cu NW electrodes were placed in a glove box and dried on a hot plate at 130 ˚C for 10 min. Then, a liquid monomer of acrylate (SR601), which was fully mixed with a photo initiator, was dropped onto the Cu NW film and cured under UV irradiation [30]. After that, the polyacrylate (PA) substrate electrode was peeled off the glass slide. The thickness of the Cu NW/PA composite electrode was controlled by a self-made mold.

The TiO_2 nanocrystals were prepared according to the method developed by Zhou et al [31]. In a typical synthesis, YCl_3 was first dissolved in 2 mL of ethanol for a final concentration of ~1 wt.%. Then, 0.5 mL of $TiCl_4$ was slowly added into the ethanol solution with stirring, followed by adding 10 mL of benzyl alcohol, resulting in a yellow solution. The solution was then heated to 80 ˚C for 5 h, forming a milky suspension. The suspension was mixed with 200 mL of diethyl ether and centrifuged to remove precipitates. The obtained product was re-dissolved in 30 mL of absolute ethanol and precipitated with the addition of 200 mL of diethyl ether, and this sequence was repeated twice. The final TiO_2 nanoparticles were collected and dispersed in ethanol to make a suspension with a concentration of 3–6 mg/mL. To stabilize the as-obtained TiO_2 solutions, titanium(IV) oxide bis(2,4-pentanedionate) ($TiO(acac)_2$) was added into the solution to a final concentration of 15 μL/mL.

2.3 Fabrication of solar cells

For the preparation of conventional solar cells, a PEDOT:PSS aqueous solution (Heraeus, Clevios PH1000) was spin-coated onto the Cu NW-polymer composite (Cu NWs/PA) electrode at 1,000 rpm for 60 s and annealed at 130 ˚C for 10 min. The thickness of the PEDOT:PSS (PH1000) layer after drying was approximately 150 nm. For conventional polymer solar cells, a PEDOT:PSS aqueous solution (Clevios™ P VP AI 4083) was spin-coated onto the Cu NW-polymer composite electrode at 3,500 rpm for 60 s and annealed at 130 ˚C for 10 min. The thickness of the PEDOT:PSS (4083) layer after drying was approximately 35 nm. The substrate was then transferred to the glove-box, and a 200-nm-thick photoactive layer was cast from a 2.5 wt.% P3HT (Rieke Metals), PCBM (American Dye Source) solution in a 1:0.8 ratio in 1,2-dichlorobenzene. The solvent dried after ~120 min in a covered petri dish. The active layer was further annealed at 130 ˚C for 10 min to completely remove the solvent. A thin layer of TiO_2 nanoparticles was spin-coated to form the electrode transfer layer. Then, the device fabrication was completed by thermal evaporation of Al (100 nm) as at the cathode under vacuum (2×10^{-3} Pa). For inverted cells, a thin layer of TiO_2 nanoparticles was spin-coated onto the Cu NW/PH1000 composite electrodes. The substrate was then transferred to the glove-box, followed by formation of a ~200 nm-thick photoactive layer (P3HT:PCBM in a 1:0.8 ratio). The solvent dried after ~120 min in a covered petri dish. The active layer was further annealed at 130 ˚C for 10 min to completely remove the solvent. Then the device fabrication was completed by the thermal evaporation of MoO_3 (10 nm) and Ag (100 nm) at the anode under vacuum (2×10^{-3} Pa).

2.4 Characterization of samples

The transmittance of the Cu NW electrodes was measured using a Lambda-950 UV-Vis spectrophotometer (PerkinElmer, Waltham, MA, USA). The Cu NW electrodes were investigated by transmission electron

microscopy (TEM, JEM-2100F, JEOL, Japan) and Raman spectroscopy (Raman DXR, Thermo Scientific, USA). The morphology of the Cu NW based electrodes and the structure of the solar cells were characterized with field emission scanning electron microscopy (FESEM, Magellan 400, FEI, USA). Surface-resistivity measurements were made using a standard four-point probe method using a Loresta-EP MCP-T 360 instrument. The bending tests were carried out with a movable-stage apparatus (ZXT_050-300_MA06, Shanghai Zhengxin Opto-Electrical Technology Co. Ltd., China). The resistance variation of the heaters was investigated by measuring the resistance of the copper contacts at the two terminals with a multimeter. The bending rate was one cycle per 2 s (0.5 Hz). The current density voltage (*J*–*V*) characteristics of the solar cells were measured using an electrochemical work station (Model CHI660C, CH) under AM1.5G illumination (100 mW/cm^2, Model YSS-80A, Yamashita). The light source was a Xe lamp equipped with an AM1.5G filter. The intensity of the incident light was 100 mW/cm^2 calibrated with a standard Si solar cell. *J*–*V* curves were recorded by a Keithley Series 2400 system source meter instrument for the stability test. A solar simulator (Newport) was used as the irradiation source to provide AM1.5G illumination for the solar cells.

3 Results and discussion

Cu NWs 60–80 nm in diameter and greater than 50 μm in length were synthesized by a modified self-catalytic method which has been used previously [26, 29]. As shown in Fig. 1(a), Cu NW films were prepared by a vacuum filtration method and transferred onto PA substrates by *in situ* polymerization to decrease the surface roughness. The as-prepared Cu NW films were nonconductive because of the oxidized layers and the residual OA on the surface. To achieve increased conductivity of the Cu NW electrodes, a TiO_2 nanoparticle sol treatment was performed before the *in-situ* polymerization. For comparison, Cu NW electrodes treated by H_2 plasma or annealing under the protection of a H_2 atmosphere were also fabricated [32]. Figure 1(b) shows the scanning electron microscopy (SEM) image of Cu NWs after TiO_2 nanoparticle sol treatment. The Cu NWs were homogenously coated by TiO_2 nanoparticles. The TEM images in Fig. 1(c) further showed the uniform coating of TiO_2. As shown in Fig. 1(d), the boundary of Cu NWs and TiO_2 can be easily distinguished in the high resolution transmission electron microscopy (HRTEM) image. No oxidized layers or residual organic matter were observed. The electron energy loss spectra in Fig. 1(e) also verified that no copper oxides were present after the TiO_2 nanoparticle treatment [33]. Figure 1(f) shows the Raman spectra of the Cu NWs before post-treatment, after H_2 plasma treatment, and after TiO_2 nanoparticle sol treatment. The Raman peak of CuO at 290 cm^{-1} disappeared after H_2 plasma treating or after TiO_2 nanoparticle sol treating. This suggested that the copper oxide layer was removed by the H_2 plasma and the TiO_2 nanoparticle sol treatments. The mechanism of H_2 plasma treating has been discussed extensively in our previous work [32]. The removal of the copper oxide layer by TiO_2 nanoparticle sol is facilitated by the residual acid of the sol which is generated during the hydrolysis of $TiCl_4$. The acid can eliminate the oxidized layers and the residual OA on the surface of Cu NWs [34, 35]. The new peak that appears at 150 cm^{-1} after the TiO_2 nanoparticle sol treatment can be assigned to TiO_2 [36]. In addition to surface cleaning, TiO_2 sol volume shrinkage and the capillary force induced by solvent evaporation resulted in tighter contacts between crossed Ag NWs and further improved film conductivity [36]. The solvent of the acidic TiO_2 sol is ethanol, which can volatilize rapidly without corroding the Cu NWs. Figure 1(g) shows the plot of the transmittance at 550 nm as a function of the sheet resistance for Cu NW films with H_2 annealing, H_2 plasma treatment, and TiO_2 nanoparticle sol treatment. Compared with H_2 annealing and H_2 plasma treating, the Cu NW films treated with the TiO_2 nanoparticle sol resulted in similar conductivity, which was better than commercial PET/ITO. Generally, the sheet resistance of the TiO_2 sol treated Cu NW electrodes were lower than 15 Ω/sq with a transmittance of 83%, while that of ITO/PET was about 35 Ω/sq at the same transmittance. The mechanical flexibility and durability of the ITO/PET and Cu NW/PA electrodes were investigated by measuring the resistance change during bending tests (10,000 cycles), as shown in Fig. 1(h). The bending rate

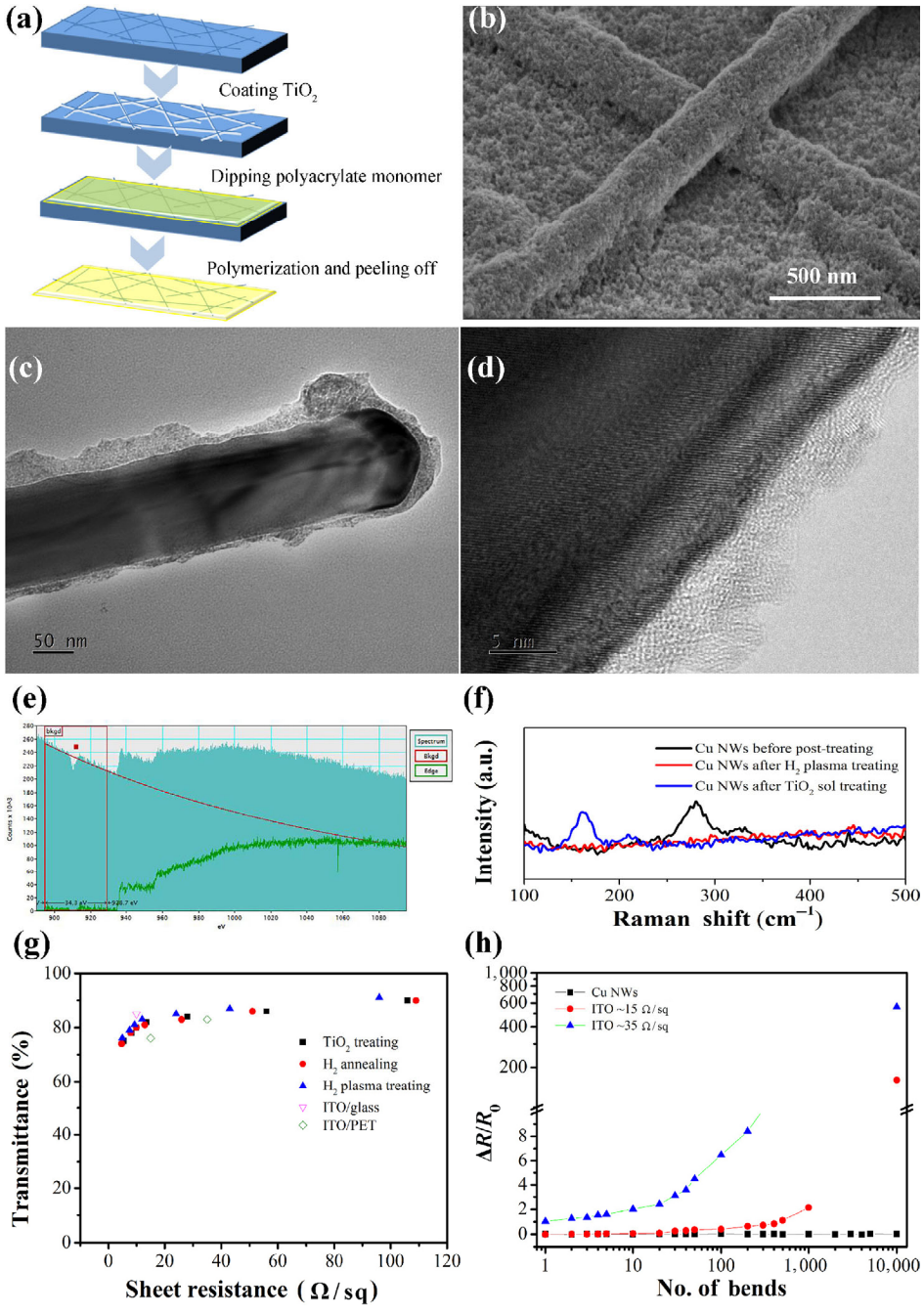

Figure 1 Schematic diagram (a) of the preparation procedure and the SEM images of the Cu NW/PA electrode. SEM (b), TEM (c), HRTEM (d), and EELS spectra (e) of the Cu NW film after TiO_2 nanoparticle sol treatment. Raman spectra (f) of the Cu NWs before post-treatment, after H_2 plasma treatment, and after TiO2 nanoparticle sol treatment. Plot of the transmittance at 550 nm as a function of sheet resistance (g) for films of Cu NWs with H_2 annealing, H_2 plasma treatment, and TiO_2 nanoparticle sol treatment. Sheet resistance variation (h) of the commercial ITO/PET and Cu NW/PA electrodes during 10,000 cycles of the bending test.

was one cycle per 2 s (0.5 Hz) and the bending radius was 3 mm. The initial sheet resistances of the Cu NW/PA electrode and ITO/PET film heaters were 13, 15 and 35 Ω/sq, respectively. The resistance variation of the PET/ITO film heater increased hundreds of thousands of times after 10,000 bending cycles. However, very slight resistance variation (<10%) was observed for the Cu NW/PA electrode after 10,000 bending cycles.

To fabricate PSCs with Cu NW electrodes, sufficient

smoothness of the Cu NW electrodes is essential. The Cu NW networks were transferred onto PA substrates by *in situ* polymerization to decrease the surface roughness. Figure 2 shows the SEM and atomic force microscope (AFM) images of the Cu NWs and Cu NW/PA electrodes. It can be seen in the SEM images that partial Cu NWs were embedded in the PA substrates. Through *in situ* polymerization, the surface of the electrodes became smoother and the surface roughness of the electrode decreased from 36.83 to 2.84 nm. It is clear that the *in-situ* polymerization and transfer of the Cu NWs decreased the surface roughness of the films sharply.

As shown in Fig. 3(a), devices with the conventional structure of PA/Cu NWs, PEDOT:PSS (PH1000), PEDOT:PSS (P VA4083), P3HT:$PC_{61}BM$, TiO_2, and Al were fabricated under optimized conditions. The current density voltage (*J*–*V*) characteristics of the PSCs based on PET/ITO and Cu NW electrodes with different post-treatment processes are shown in Fig. 3(b). The photovoltaic parameters of the devices are summarized in Table 1. For the cells based on ITO/PET electrodes, PCEs of 2.69% and 2.46%, with both V_{OC} = 0.57 V, J_{SC} = 8.70 and 8.42 mA/cm^2, FF = 58.0% and 56.5% were obtained with sheet resistances of 35 Ω/sq (83% T) and 15 Ω/sq (76% T). V_{OC}: open-circuit voltage; J_{SC}: short-circuit current density; FF: fill factor. The higher J_{SC} is likely due to greater transparency,

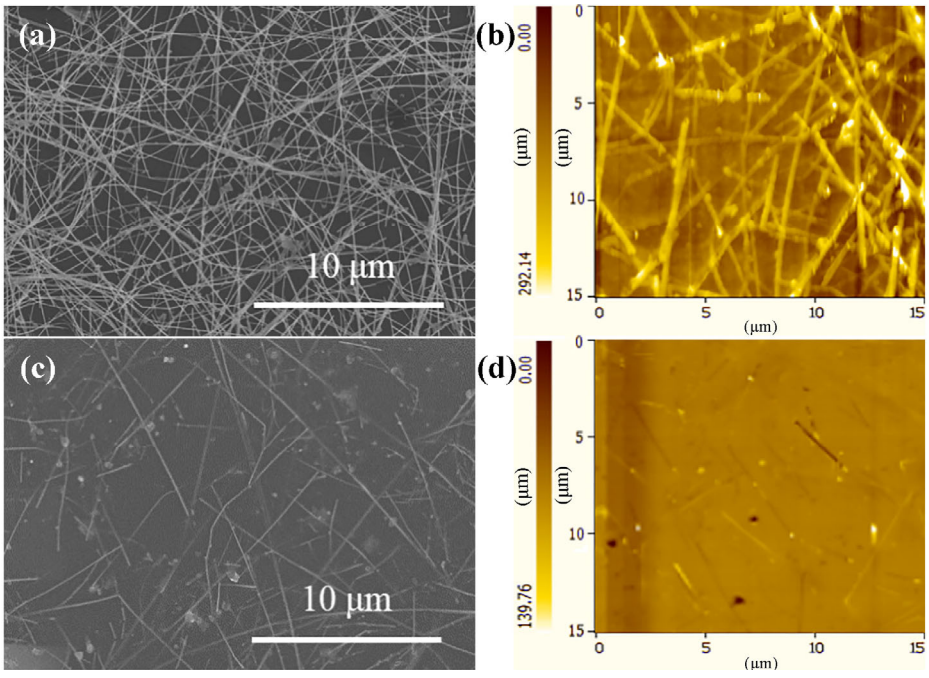

Figure 2 SEM images ((a) and (c)) and AFM images ((b) and (d)) of the Cu NWs ((a) and (b)) and Cu NW/PA electrode ((c) and (d)).

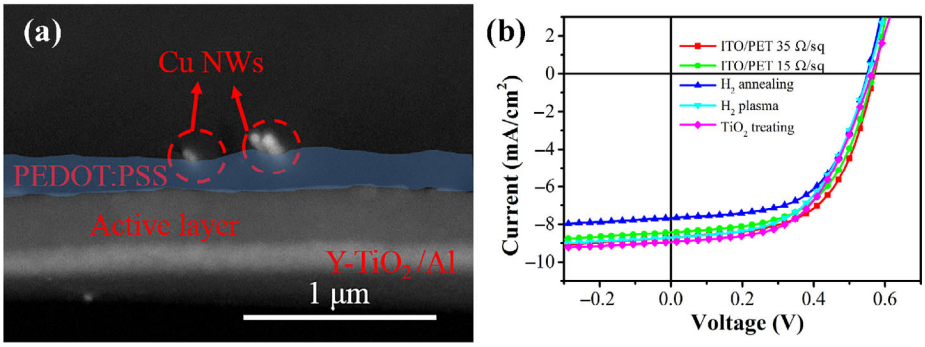

Figure 3 Cross-section SEM image (a) of the conventional PSCs based on Cu NW/PA electrodes. *J*–*V* curve (b) of the flexible PSCs based on ITO and Cu NW electrodes with different post-treatment processes.

Table 1 Photovoltaic parameters of conventional PSCs based on ITO and Cu NW electrodes with different post-treatment processes

	J_{SC} (mA/cm^2)	V_{OC} (V)	FF (%)	η (%)
ITO/PET 35 Ω/sq	8.70	0.57	58.0	2.69
ITO/PET 15 Ω/sq	8.42	0.57	56.5	2.46
H_2 annealing	7.70	0.55	56.5	2.39
H_2 plasma	8.91	0.54	53.9	2.61
TiO_2 treating	8.92	0.56	54.4	2.71

Table 2 Photovoltaic parameters of the inverted PSCs based on ITO and Cu NW electrodes with different post-treatment processes

	J_{SC} (mA/cm^2)	V_{OC} (V)	FF (%)	η (%)
ITO/PET 35 Ω/sq	8.34	0.57	58	2.75
ITO/PET 15 Ω/sq	7.35	0.56	54	2.22
H_2 annealing	8.91	0.60	52	2.83
H_2 plasma	9.88	0.60	53	3.14
TiO_2 treating	9.63	0.60	51	3.11

which led to a higher PCE. The device based on Cu NW electrodes with TiO_2 treatment (13 Ω/sq @ 82% T) showed the highest PCE (η = 2.71%, V_{OC} = 0.56 V, J_{SC} = 8.92 mA/cm^2, and FF = 54.4%) compared with the devices prepared with H_2 annealing (PCE: 2.39%) and H_2 plasma treatment (PCE: 2.61%). This can be mainly attributed to the protection of the uniform TiO_2 coating. The acidic PEDOT:PSS solution corrodes the Cu NWs during the spin-coating and drying processes, which would decrease the conductivity of the electrodes [23]. The uniform coating of TiO_2 may help to prevent the acidic solution from damaging the Cu NW conductive network.

Devices with the inverted structures of PA/Cu NWs, PEDOT:PSS (PH1000), TiO_2, P3HT:PC_{61}BM, MoO_3, and Ag were also fabricated under optimized conditions, as shown in Fig. 4(a). The current density voltage characteristics of the PSCs based on PET/ITO and Cu NW electrodes with different post-treatment processes are shown in Fig. 4(b). The photovoltaic parameters of the devices are summarized in Table 2. For the ITO/PET electrode based cells, PCEs of 2.75% and 2.22%, with V_{OC} = 0.57 and 0.56 V, J_{SC} = 8.34 and 7.35 mA/cm^2, and FF = 58% and 54% were obtained with sheet resistances of 35 and 15 Ω/sq. The device based on Cu NW electrodes with TiO_2 treatment showed a PCE of 3.11% (with V_{OC} = 0.60 V, J_{SC} = 9.63 mA/cm^2, and FF = 51%), which was comparable to the devices treated with H_2 plasma (η = 3.14%, V_{OC} = 0.60 V, J_{SC} = 9.88 mA/cm^2, and FF = 53%), but much higher than the devices treated by H_2 annealing (η = 2.83%, V_{OC} = 0.60 V, J_{SC} = 8.91 mA/cm^2, and FF = 52%) and the PET/ ITO based devices. Compared with conventional solar cells, inverted cells with Cu NW electrodes achieved higher PCEs. Conversely, PET/ITO devices exhibited almost the same performance between conventional and inverted cells. For conventional cells, the acidic PEDOT:PSS (P VP AI 4083) solution was spin-coated after spin-coating PEDOT:PSS (PH1000). The longer contact time of the Cu NWs with the acidic PEDOT:PSS solution would lead to more serious damage of the Cu NW network, thus affecting the electron collection ability of the cells.

The mechanical flexibility of the solar cells was investigated by measuring the performance change of the cells during bending tests (500 cycles), as shown in Fig. 5. The bending rate was about one cycle per 2 s (0.5 Hz) and the bending radius was 3 mm. The PCE

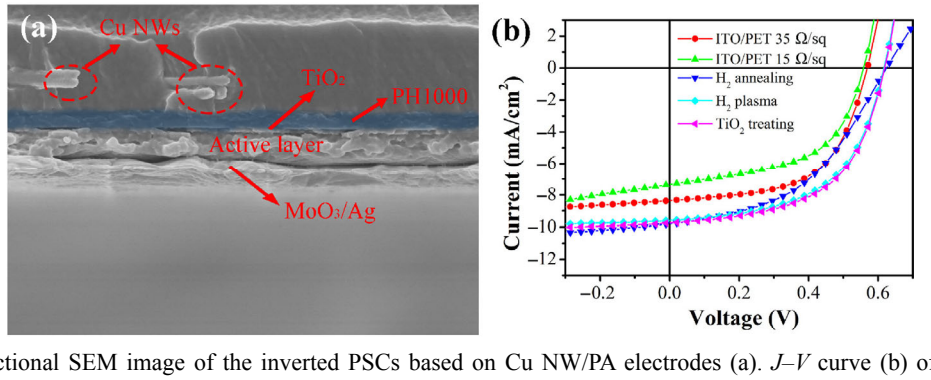

Figure 4 Cross-sectional SEM image of the inverted PSCs based on Cu NW/PA electrodes (a). *J*–*V* curve (b) of the flexible PSCs based on ITO and Cu NW electrodes with different post-treatment processes.

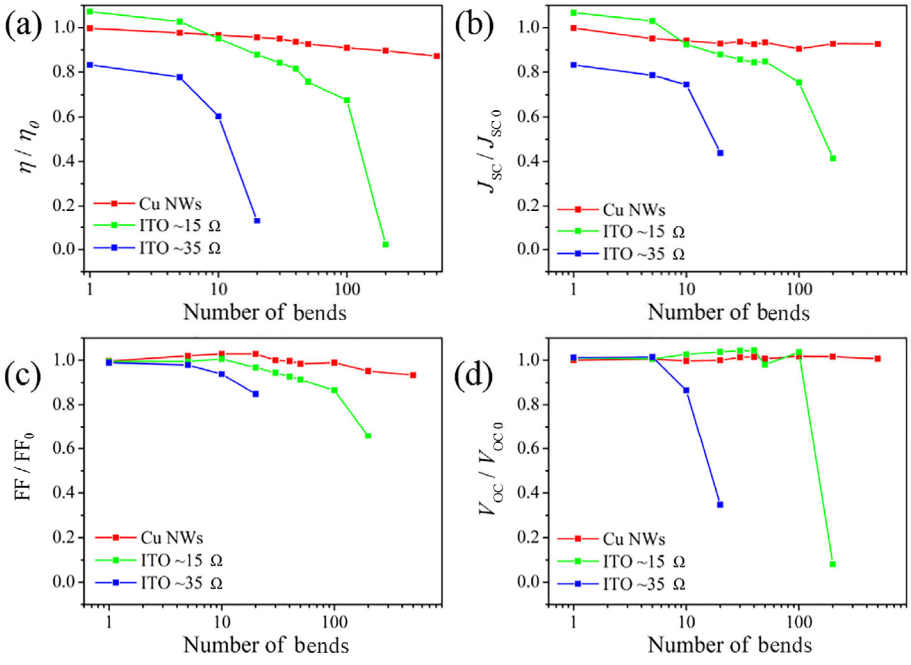

Figure 5 The PCE (a), current density (b), fill factor (c), and open-circuit voltage (d) variation of the flexible PSCs based on ITO/PET and Cu NW/PA electrodes during the bending test.

of the PET/ITO based cells decreased by 90 percent after 20 (with sheet resistance of 35 Ω/sq) and 200 (with sheet resistance of 15 Ω/sq) bending cycles. In contrast, there was hardly any conversion efficiency variation (<10%) observed for the Cu NW electrode based cells even after 500 bending cycles. The performance change of the cells was roughly in line with the trend of sheet resistance. This indicated that the sheet resistance variation is one of the most important factors responsible for the failure of cells during the bending test. The increased sheet resistance results in tremendous internal resistance and decreased current density. The decreased fill factor and open-circuit voltage can be ascribed to structural damage of the cells that occurs upon repeated bending.

4 Conclusions

In this work, we developed a TiO_2 nanoparticle sol treatment process to achieve Cu NW based transparent electrodes with high conductivity at room temperature. Conventional and inverted PSCs based on the Cu NW electrodes were fabricated. The factors crucial for achieving ideal electronic properties during the cell fabrication process were discussed in detail. Inverted cells based on Cu NW electrodes exhibited a PCE of 3.11% with a P3HT:PC_{61}BM blend film as the active layer, which is much better than commercial PET/ITO. In addition, solar cells based on Cu NW electrodes showed excellent flexibility (90% of the PCE retained after 500 bending test cycles) compared with cells based on ITO/PET, which failed after 20 and 200 bending cycles at sheet resistances of 35 and 15 Ω/sq, respectively.

Acknowledgements

This work was financially supported by the National Natural Science Foundation of China (No. 61301036), Shanghai science and Technology Star Project (No. 17QA1404700), Youth Innovation Promotion Association CAS (No. 2014226), Shanghai Key Basic Research Project (No. 16JC1402300), and the Major State Research Development Program of China (No. 2016YFA0203000).

References

[1] Lucera, L.; Machui, F.; Kubis, P.; Schmidt, H. D.; Adams, J.; Strohm, S.; Ahmad, T.; Forberich, K.; Egelhaaf, H.-J.; Brabec C. J. Highly efficient, large area, roll coated flexible and

rigid OPV modules with geometric fill factors up to 98.5% processed with commercially available materials. *Energy Environ. Sci.***2016**, *9*, 89–94.

[2] Tait, J.G.; Merckx, T.; Li, W. Q.; Wong, C.; Gehlhaar, R.; Cheyns, D.; Turbiez, M.; Heremans, P. Blade coating: Determination of solvent systems for blade coating thin film photovoltaics *Adv. Funct. Mater.* **2015**, *25*, 3444.

[3] Tait, J.G.; Merckx, T.; Li, W. Q.; Wong, C.; Gehlhaar, R.; Cheyns, D.; Turbiez, M.; Heremans, P. Determination of solvent systems for blade coating thin film photovoltaics. *Adv. Funct. Mater.* **2015**, *25*, 3393–3398.

[4] Guo, F.; Kubis, P.; Przybilla, T.; Spiecker, E.; Hollmann, A.; Langner, S.; Forberich, K.; Brabec, C. J. Nanowire interconnects for printed large-area semitransparent organic photovoltaic modules. *Adv. Energy Mater.* **2015**, *5*, 1401779.

[5] Nyman, M.; Dahlström, S.; Sandberg, O. J.; Österbacka, R. Unintentional bulk doping of polymer-fullerene blends from a thin interfacial layer of MoO_3. *Adv. Energy Mater.* **2016**, *6*, 1600670.

[6] Li, S. S.; Ye, L.; Zhao, W. C.; Zhang, S. Q.; Mukherjee, S.; Ade, H.; Hou, J. H. Energy-level modulation of small-molecule electron acceptors to achieve over 12% efficiency in polymer solar cells. *Adv. Mater.***2016**, *28*, 9423–9429.

[7] Zhong, W.; Chen, L.; Xiao, S. Q.; Huang, L. Q.; Chen, Y. W. A versatile buffer layer for polymer solar cells: Rendering surface potential by regulating dipole. *Adv. Funct. Mater.* **2015**, *25*, 3164–3171.

[8] Zhang, K.; Hu, Z. C.; Xu, R. G.; Jiang, X. F.; Yip, H. L.; Huang, F.; Cao, Y. High-performance polymer solar cells with electrostatic layer-by-layer self-assembled conjugated polyelectrolytes as the cathode interlayer. *Adv. Mater.* **2015**, *27*, 3607–3613.

[9] Shim, H.-S.; Lin, F.; Kim, J.; Sim, B.; Kim, T. M.; Moon, C. K.; Wang, C. K.; Seo, Y.; Wong, K. T.; Kim, J. J. Efficient vacuum-deposited tandem organic solar cells with fill factors higher than single-junction subcells. *Adv. Energy Mater.* **2015**, *5*, 1500228.

[10] Ham, J.; Dong, W. J.; Park, J. Y.; Yoo, C. J.; Lee, I.; Lee, J. L. A challenge beyond bottom cells: Top-illuminated flexible organic solar cells with nanostructured dielectric/metal/polymer (DMP) films. *Adv. Mater.* **2015**, *27*, 4027–4033.

[11] Choi, H.; Ko, S. J.; Kim, T.; Morin, P. O.; Walker, B.; Lee, B. H.; Leclerc, M.; Kim, J. Y.; Heeger, A. J. Small-bandgap polymer solar cells with unprecedented short-circuit current density and high fill factor. *Adv. Mater.* **2015**, *27*, 3318–3324.

[12] Smith, A. J.; Wang, C.; Guo, D. N.; Sun, C.; Huang, J. X. Repurposing Blu-ray movie discs as quasi-random nanoim-printing templates for photon management. *Nat. Commun.* **2014**, *5*, 5517.

[13] Yao, K.; Xin, X. K.; Chueh, C. C.; Chen, K. S.; Xu, Y. X.; Jen, A. K.Y. Enhanced light-harvesting by integrating synergetic microcavity and plasmonic effects for high-performance ITO-free flexible polymer solar cells. *Adv. Funct. Mater.* **2015**, *25*, 567–574.

[14] dos Reis Benatto, G.A.; Roth, B.; Corazza, M.; Søndergaard, R. R.; Gevorgyan, S. A.; Jørgensena, M.; Krebs, F. C. Roll-to-roll printed silver nanowires for increased stability of flexible ITO-free organic solar cell modules. *Nanoscale* **2015**, *8*, 318–326.

[15] Mao, L.; Chen, Q.; Li, Y. W.; Li, Y.; Cai, J. H.; Su, W. M.; Bai, S.; Jin, Y. Z.; Ma, C. Q.; Cui, Z. et al. Flexible silver grid/PEDOT:PSS hybrid electrodes for large area inverted polymer solar cells.*Nano Energy* **2014**, *10*, 259–267.

[16] Kim, S.; Sanyoto, B.; Park, W. T.; Kim, S.; Mandal, S.; Lim, J. C.; Noh, Y. Y.; Kim, J. H. Ultrafiltration: Purification of PEDOT:PSS by ultrafiltration for highly conductive transparent electrode of all-printed organic devices (Adv. Mater. 46/2016). *Adv. Mater.***2016**, *28*, 10106–10106.

[17] Wang, R. R.; Sun, J.; Gao, L.; Zhang, J. Base and acid treatment of SWCNT-RNA transparent conductive films. *ACS Nano* **2010**, *4*, 4890–4896.

[18] Bae, S.; Kim, H.; Lee, Y.; Xu, X. F.; Park, J. S.; Zheng, Y.; Balakrishnan, J.; Lei, T.; Ri, K. H.; Song, Y. I. et al. Roll-to-roll production of 30-inch graphene films for transparent electrodes. *Nat. Nanotechnol.* **2010**, *5*, 574–578.

[19] Ning, J.; Hao, L.; Jin, M. H.; Qiu, X. Y.; Shen, Y. D.; Liang, J. X.; Zhang, X. H.; Wang, B.; Li, X. L.; Zhi, L. J. A facile reduction method for roll-to-roll production of high performance graphene-based transparent conductive films. *Adv. Mater.* **2016**, *29*, 1605028.

[20] Liang, J. J.; Li, L.; Tong, K.; Ren, Z.; Hu, W.; Niu, X. F.; Chen, Y. S.; Pei, Q. B. Silver nanowire percolation network soldered with graphene oxide at room temperature and its application for fully stretchable polymer light-emitting diodes. *ACS Nano* **2014**, *8*, 1590–1600.

[21] Sung, H.; Ahn, N.; Jang, M. S.; Lee, J. K.; Yoon, H.; Park, N. G.; Choi, M. Transparent conductive oxide-free graphene-based perovskite solar cells with over 17% efficiency. *Adv. Energy Mater.* **2015**, *6*, 1501873.

[22] Song, M.; You, D. S.; Lim, K.; Park, S.; Jung, S.; Kim, C. S.; Kim, D. H.; Kim, D. G.; Kim, J. K.; Park, J. et al. Highly efficient and bendable organic solar cells with solution-processed silver nanowire electrodes. *Adv. Funct. Mater.* **2013**, *23*, 4177–4184.

[23] Sachse, C.; Weiß, N.; Gaponik, N.; Müller-Meskamp, L.; Eychmüller, A.; Leo, K. ITO-free, small-molecule organic solar cells on spray-coated copper-nanowire-based transparent electrodes. *Adv. Energy Mater.* **2014**, *4*, 1300737.

[24] Li, L.; Yu, Z. B.; Hu, W. L.; Chang, C. H.; Chen, Q.; Pei, Q. B. Efficient flexible phosphorescent polymer light-emitting diodes based on silver nanowire-polymer composite electrode. *Adv. Mater.* **2011**, *23*, 5563–5567.

[25] Chen, J. Y.; Zhou, W. X. Chen, J.; Fan, Y.; Zhang, Z. Q.; Huang, Z. D.; Feng, X. M.; Mi, B. X.; Ma, Y. W.; Huang, W. Solution-processed copper nanowire flexible transparent electrodes with PEDOT:PSS as binder, protector and oxide-layer scavenger for polymer solar cells. *Nano Res.* **2015**, *8*, 1017–1025.

[26] Zhang, D. Q.; Wang, R. R.; Wen, M. C.; Weng, D.; Cui, X.; Sun, J.; Li, H. X.; Lu, Y. F. Synthesis of ultralong copper nanowires for high-performance transparent electrodes. *J. Am. Chem. Soc.* **2012**, *134*, 14283–14286.

[27] Zhai, H. T.; Wang, R. R.; Wang, W. Q.; Wang, X.; Cheng, Y.; Shi, L. J.; Liu, Y. Q.; Sun, J. Novel fabrication of copper nanowire/cuprous oxidebased semiconductor-liquid junction solar cells. *Nano Res.* **2015**, *8*, 3205–3215.

[28] Cheng, Y.; Wang, R. R.; Sun, J.; Gao, L. A stretchable and highly sensitive graphene-based fiber for sensing tensile strain, bending, and torsion. *Adv. Mater.* **2015**, *27*, 7365–7371.

[29] Zhai, H. T.; Wang, R. R.; Wang, X.; Cheng, Y.; Shi, L. J.; Sun, J. Transparent heaters based on highly stable Cu nanowire films. *Nano Res.* **2016**, *9*, 3924–3936.

[30] Wang, S. L.; Cheng, Y.; Wang, R. R.; Sun, J.; Gao, L. Highly thermal conductive copper nanowire composites with ultralow loading: Toward applications as thermal interface materials. *ACS Appl. Mater. Interfaces* **2014**, *6*, 6481–6486.

[31] Zhou, H.P.; Chen, Q.; Li, G.; Luo, S.; Song, T. B.; Duan, H. S.; Hong, Z. R.; You, J. B.; Liu, Y. S.; Yang, Y. Interface engineering of highly efficient perovskite solar cells. *Science* **2014**, *345*, 542–546.

[32] Wang, R. R.; Zhai, H. T.; Wang, T.; Wang, X.; Cheng, Y.; Shi, L. J.; Sun, J. Plasma-induced nanowelding of a copper nanowire network and its application in transparent electrodes and stretchable conductors. *Nano Res.* **2016**, *9*, 2138–2148.

[33] Thiel, B. L.; Sarikaya, M. Electron energy loss spectroscopy of copper-oxygen systems at the Cu L-edge. *Phys. B: Cond. Matter* **1989**, *158*, 568–571.

[34] Won, Y.; Kim, A.; Lee, D.; Yang, W.; Woo, K.; Jeong, S.; Moon, J. Annealing-free fabrication of highly oxidation-resistive copper nanowire composite conductors for photovoltaics. *NPG Asia Mater.* **2014**, *6*, e105.

[35] Wang, X.; Wang, R. R.; Zhai, H. T.; Shen, X.; Wang, T.; Shi, L. J.; Yu, R. C.; Sun, J. Room-temperature surface modification of Cu nanowires and their applications in transparent electrodes, SERS-based sensors, and organic solar cells. *ACS Appl. Mater. Interfaces* **2016**, *8*, 28831–28837.

[36] Xue, X. X.; Ji, W.; Mao, Z.; Mao, H. J.; Wang, Y.; Wang, X.; Ruan, W. D.; Zhao, B.; Lombardi, J. R. Raman investigation of nanosized TiO_2: Effect of crystallite size and quantum confinement. *J. Phys. Chem. C* **2012**, *116*, 8792–8797.